Journal of Magnetism and Magnetic Materials 419 (2016) 98–104

Contents lists available at ScienceDirect

Journal of Magnetism and Magnetic Materials

journal homepage: www.elsevier.com/locate/jmmm

Surface magnetic contribution in zinc ferrite thin films studied by element- and site-specific XMCD hysteresis-loops

P. Mendoza Zélis [a,b], G.A. Pasquevich [a,b], K.L. Salcedo Rodríguez [a], F.H. Sánchez [a], C.E. Rodríguez Torres [a,*]

[a] IFLP-CCT-La Plata-CONICET and Departamento de Física, Facultad de Ciencias Exactas, C. C. 67, Universidad Nacional de La Plata, 1900 La Plata, Argentina
[b] Departamento de Ciencias Básicas, Facultad de Ingeniería, Universidad Nacional de La Plata, 1900 La Plata, Argentina

ARTICLE INFO

Article history:
Received 31 July 2015
Received in revised form
27 May 2016
Accepted 31 May 2016
Available online 4 June 2016

Keywords:
Maghemite nanoparticles
Zinc ferrite
XMCD hysteresis-loops
Surface anisotropy

ABSTRACT

Element- and site-specific magnetic hysteresis-loops measurements on a zinc ferrite ($ZnFe_2O_4$) thin film were performed by X-ray magnetic circular dichroism. Results show that iron in octahedral and tetrahedral sites of spinel structure are coupled antiferromagnetically between them, and when magnetic field is applied the magnetic moment of the ion located at octahedral sites aligns along the field direction. The magnetic measurements reveal a distinctive response of the surface with in-plane anisotropy and an effective anisotropy constant value of 12.6 kJ/m^3. This effective anisotropy is due to the combining effects of demagnetizing field and, volume and surface magnetic anisotropies $K_V = 3.1$ kJ/m^3 and $K_S = 16$ μJ/m^2.

1. Introduction

It is well known that the disordered distribution of zinc and iron ions in $ZnFe_2O_4$ leads to a drastic change in its magnetic order [1–3]. This phenomenon makes $ZnFe_2O_4$ one of the most studied magnetic ferrites. This compounds has an spinel structure were its smallest cell has cubic symmetry. The iron atoms occupy the so called A- and B-sites located in tetrahedral and the octahedral sites which are surrounded by 4 and 6 oxygen atoms [4]. $ZnFe_2O_4$ has an antiferromagnetic order below the Néel temperature $T_N = 10.5$ K [5], which is driven by an oxygen-mediated super-exchange between the Fe^{3+} ions located at the octahedral B-sites (Fe_B^{3+}). Nanosized $ZnFe_2O_4$ samples, whether as nanoparticles [1,6] or as thin films [7–10] display ferrimagnetic behavior at room temperature. This ferrimagnetic feature is attributed to the distribution of Fe^{3+} and Zn^{2+} at both tetrahedral A- and octahedral B-sites which gives rise to strong negative J_{AB} interactions. The fact that ferrimagnetic behavior is detected in nanometric systems indicates that the phenomenon may be related with surfaces.

In a recent work [11] we have demonstrated that the large magnetic moment observed in zinc ferrite thin films grown at low oxygen pressure is due to the ferromagnetic coupling between iron ions occupying B-sites. The reason for this is based on three main mechanisms that break the original antiferromagnetic interaction between B-sites, namely, the A-site overpopulation, the consequent generation of octahedral cation vacancies, and the existence of an oxygen vacancy between two Fe_B ions.

In this work we present a study of the surface magnetic anisotropy of zinc ferrite ($ZnFe_2O_4$) thin films (thickness $t \sim 57$ nm) grown at low O_2 pressure for which we have performed measurements of magnetic hysteresis via X-ray Magnetic Circular Dichroism (XMCD).

XMCD is an element- and site-specific selective technique that allows to discern among the magnetic contributions of non-equivalent atomic sites [12–16]. The XMCD spectrum is defined as the difference between two X-ray absorption spectra (XAS), one measured with the circular polarization vector parallel and other antiparallel to the external magnetic field. The XMCD signal can be also obtained in an equivalent procedure by illuminating the sample with one polarization (left or right) and inverting the applied magnetic field direction (parallel or anti-parallel to the direction of the light propagation).

XMCD signal is obtained at inner shell absorption edges where electronic transitions between core states and unoccupied valence states occur. In transition metals such as Fe, Ni and Co, the largest contribution to the XMCD signal involves $p \rightarrow d$ dipole transitions (core $p_{1/2}$ and $p_{3/2}$ electrons $\rightarrow$ unoccupied d valence states). The XMCD signal is proportional to the difference between the spin-up and spin-down occupations of the unoccupied d states in the valence levels of the absorbing atoms. This means that XMCD is able to probe magnetic properties of a specific absorbing element. In

* Corresponding author.
E-mail address: torres@fisica.unlp.edu.ar (C.E. Rodríguez Torres).

http://dx.doi.org/10.1016/j.jmmm.2016.05.105
0304-8853/

some cases it is also possible to distinguish the magnetic behavior between different chemical states or crystallographic sites of the atoms of one chemical species, depending on the element and on the energy resolution of the beamline.

The intensity of XMCD signal is proportional to the mean magnetic moment projected onto the direction of the incident X-ray, and its sign reveals the direction of the probed moment in relation to the direction of the incident photon [17]. For atomic magnetic moments oriented parallel to the external magnetic field, the XMCD is negative at the L3 edge and positive at the L2 edge [18].

Since contributions of Fe^{3+} in A- and B-sites in spinel structure are clearly distinguishable from each other in XMCD signals [11], hysteresis-loops for each iron site can be obtained measuring the X-ray absorption as a function of the magnetic field intensity at different characteristic energies.

The most common and convenient method for measuring the absorption cross section in XAS is through total electron yield (TEY). A soft X-ray photon absorbed by a material generates an atomic core hole. Auger is the dominant decay process. The TEY mode detects the secondary electrons generated by the inelastic scattering of Auger.

XMCD in the TEY is proportional to an average near-surface magnetic moment because the measured signal is weighted by an exponential function with a decay length (mean free escape depth of electrons emitted from the surface) of a few nanometers. Thus, with this technique is possible to determine the surface magnetic contribution since its mean probing depth is few nanometers.

In this work we study the surface magnetic contribution in zinc ferrite thin film by XMCD in the TEY mode and analyze the results in terms of the surface magnetic anisotropy. Also, for testing purposes we made the same measurements on maghemite γ-Fe_2O_3 nanoparticles.

2. Experimental details

The zinc ferrite ($ZnFe_2O_4$) thin film, hereafter labeled ZFO1 as in references [9,11], has a thickness of 57 nm and an area of 5 mm × 5 mm. It was grown at low O_2 pressure (10^{-5} mbar). Details of sample preparation and characterization can be found elsewhere [9]. For comparison purposes, we have also measured maghemite (γ-Fe_2O_3) nanoparticles with 15 nm of radii.

X-ray absorption spectroscopy (XAS) experiments at $L_{2,3}$ edges of iron were performed at room temperature at PGM beamline [19] of Brazilian Synchrotron Light Laboratory-LNLS (Campinas, Brazil) using circularly polarized light with a degree of circular polarization around 80%. The absorption data were collected in the TEY mode. The photon beam and the magnetic field were perpendicular to the sample plane. The base pressure of the system was 10^{-10} mbar. The absorption was normalized to the incoming photon beam intensity by measuring simultaneously the photocurrent at a gold grid. The magnetic field strength $\mu_0\mathbf{H}$ (between −0.6 and 0.6 T) was generated by an electromagnet. All measurements were made at 290 K. The maghemite γ-Fe_2O_3 nanoparticles were measured dispersed in double-sided conductive carbon tape.

The absorption cross section of the circular polarized X-rays is labeled $\mu^{\alpha\beta}$, where α denotes the helicity of the photon ($\alpha=\uparrow(\downarrow)$ when the photon is right-handed (left-handed) polarized) and β denotes the direction of the magnetic field ($\beta=\uparrow(\downarrow)$ when the magnetic field is parallel (antiparallel) to the propagation vector). In the electric dipole approximation, reversing the magnetic field is equivalent to changing beam helicity, thus $\mu^{\uparrow\uparrow}=\mu^{\downarrow\downarrow}$ and $\mu^{\uparrow\downarrow}=\mu^{\downarrow\uparrow}$. The XMCD signal is the difference $\mu^{\uparrow\uparrow}-\mu^{\uparrow\downarrow}$. To compensate systematic uncertainties inherent to the measurement process of the absorption cross section, the XMCD signal was obtained as: $\mu_{XMCD}=(\mu^{\uparrow\uparrow}+\mu^{\downarrow\downarrow}-\mu^{\uparrow\downarrow}-\mu^{\downarrow\uparrow})/2$.

XMCD signal is a function of the magnetic field intensity since this signal is proportional to the mean magnetic moment projected onto the direction of the incident X-ray, which in our case is the same of the magnetic field. In this sense, it is possible to measure the mean magnetic moment projection on the magnetic field direction as a function of the intensity of the latter. This kind of measurement is called XMCD hysteresis-loops.

XMCD hysteresis-loops were recorded by setting the photon energy at specific energies (maximum or minimum of L_3-edge XMCD signal) and measuring the absorption intensity $I_L(H)$ and $I_R(H)$ with left and right circularly polarized light while sweeping the magnetic field strength at a velocity of 6.2×10^{-3} T/s, back and forth, between −0.6 T and 0.6 T. Each complete magnetic cycle (at a specific energy) was repeated eight times and then an average was performed to obtain $I_R(H)$ and $I_L(H)$. Then, the XMCD hysteresis-loops were obtained as $I_R(H)$–$I_L(H)$. The positive (negative) values of $\mu_0 H$ correspond to magnetic field parallel (antiparallel) to the propagation vector direction. The origin of the ordinate is determined from the symmetry of each hysteresis-loop.

Conventional hysteresis-loops (magnetization as a function of applied magnetic field) were obtained using vibrating sample magnetometer (VSM) LakeShore 7404 operated at 290 K with maximum magnetic field strength $\mu_0\mathbf{H}$ = 0.6 T. Maghemite nanoparticles were measured dispersed in double-sided tape as in the XMCD experiments. Zinc ferrite thin film was measured with the applied magnetic field both parallel and perpendicular to the film plane.

3. Results and discussion

Figs. 1a and 2a show the XAS $L_{2,3}$ spectra $\mu^+=(\mu^{\uparrow\uparrow}+\mu^{\downarrow\downarrow})/2$ and $\mu^-=(\mu^{\uparrow\downarrow}+\mu^{\downarrow\uparrow})/2$ under a magnetic field strength of $\mu_0 H=0.6$ T corresponding to maghemite nanoparticles and ZFO1 samples, respectively. They present the typical features corresponding to the 2*p* to 3*d* electronic transitions [20]. From this spectrum it is possible to obtain the total magnetic moment per iron atom by using sum rules [17]. The values obtained at 0.6 T are 0.80 and 0.93 μ_B/Fe for maghemite nanoparticles and ZFO1 film, respectively [11].

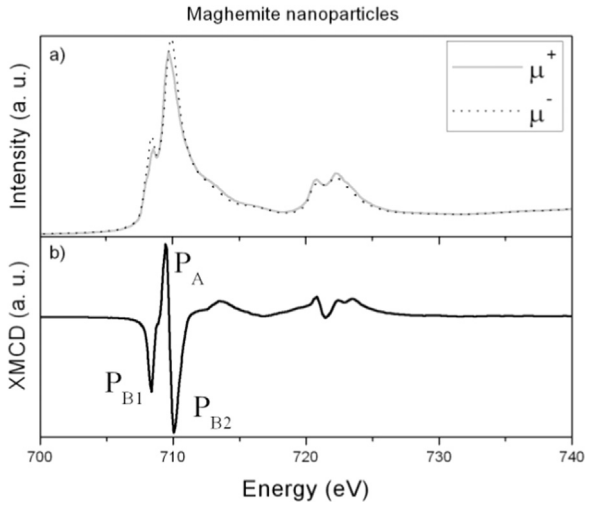

Fig. 1. a) XAS $L_{2,3}$ spectra corresponding to maghemite nanoparticles under an magnetic field strength of $\mu_0 H=0.6$ T. $\mu^+=(\mu^{\uparrow\uparrow}+\mu^{\downarrow\downarrow})/2$ and $\mu=(\mu^{\uparrow\downarrow}+\mu^{\downarrow\uparrow})/2$. b) XMCD signals of maghemite nanoparticles. Positive peak P_A at 709 eV can be assigned to magnetic contributions from Fe_A^{3+} while the two negative peaks P_{B1} and P_{B2} at 708 and 710 eV can be assigned to Fe_B^{3+} ions.

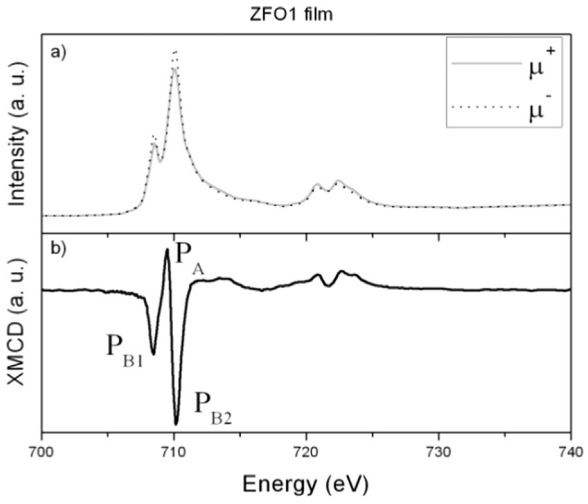

Fig. 2. a) XAS $L_{2,3}$ spectra corresponding to ZFO1 film under an magnetic field strength of $\mu_0 H = 0.6$ T. $\mu^+ = (\mu^{\uparrow\uparrow} + \mu^{\downarrow\downarrow})/2$ and $\mu^- = (\mu^{\uparrow\downarrow} + \mu^{\downarrow\uparrow})/2$. b) XMCD signals of ZFO1 film. Positive peak P_A at 709 eV can be assigned to magnetic contributions from Fe_A^{3+} while the two negative peaks P_{B1} and P_{B2} at 708 and 710 eV can be assigned to Fe_B^{3+} ions.

Figs. 1b and 2b exhibit the XMCD signal of maghemite nanoparticles and ZFO1 samples, respectively. Although both XMCD signals derive from the superposition of contributions from Fe^{3+} at A- and B-sites, they allow to distinguishing the contribution from each site [18]. Results show that the XMCD signals at L_3-edge of both samples consist of a positive peak P_A at about 709 eV and two negative peaks P_{B1} and P_{B2} at 708 and 710 eV, respectively (Fig. 2). Inspecting the Fe^{3+} at A-sites and B-sites contributions at these energies on XAS, each peak can be assigned to one site. The P_A peak can be assigned to magnetic contributions from Fe^{3+} at A-sites (Fe_A^{3+}) while P_{B1} and P_{B2} are related to Fe^{3+} at B-sites (Fe_B^{3+}). Fe_A^{3+} ions are antiferromagnetically coupled to Fe_B^{3+}. When applying a magnetic field the Fe_B^{3+} ion moments align along the field direction, while Fe_A^{3+} ones orient opposite to the field. This configuration gives rise to positive and negative dichroic signals at L_3 edge for Fe_A^{3+} and Fe_B^{3+}, respectively [18].

In order to obtain XMCD hysteresis-loops of Fe^{3+} both at A- and B-sites, the X-ray energy was fixed at the maximum (or minimum) of P_A, P_{B1} and P_{B2} peaks (see Figs. 1a and 2a) while $I_R(H)$ and $I_L(H)$ signals were measured. For control purpose, the same measurements were made at 700 eV (off-resonance or background) were no XMCD signal dependence on magnetic field is expected. In Fig. 3a the $I_R(H)$ and $I_L(H)$ signals for X-ray energy fixed at 708 eV (P_{B1} Peak) and at 700 eV (off-resonance) for ZFO1 film are shown. The undesirable dependence of the absorption intensity at 700 eV with the applied magnetic field is because emitted electrons are influenced by the magnetic field intensity [16]. The procedure used in this work to obtain the XMCD hysteresis-loops resolves this fact as can be noted in Fig. 3b, where no dependence of the XMCD intensity on the applied field is observed at 700 eV (off-resonance). In this figure the XMCD hysteresis-loops obtained as $I_R(H)$–$I_L(H)$ for both P_{B1} and off-resonance are shown. Positive (negative) values of $\mu_0 H$ correspond to magnetic field parallel (antiparallel), and thin (thick) lines correspond to experiment performed from negative to positive (positive to negative) values of $\mu_0 H$.

Figs. 4a and 5a show the loops recorded for each peak of maghemite nanoparticles and ZFO1 samples, respectively. All loops were normalized by the XMCD intensity value at 0.6 T of P_{B2} peak for each sample. In the case of the ZFO1, the sample plane is perpendicular to the direction of the photon propagation-vector and of the magnetic field.

Fig. 4b presents the XMCD hysteresis-loops and the VSM hysteresis-loops of maghemite nanoparticles, all of them normalized by their values at 0.6 T. It can be seen that all XMCD curves coincide. The mean magnetic moment projection of the Fe^{3+} ion in the A-site flips at $\mu_0 H \leq 0.02$ T in good agreement with the coercive field measured by VSM. The signal saturates at $\mu_0 H \sim 0.5$ T together with those of the Fe ions in the B-site. All the XMCD hysteresis-loops characteristics are in very good agreement with the corresponding curve obtained by VSM. Because of nanometric size of particles, both techniques reveal the same magnetic response, despite the fact that VSM technique is sensitive to the whole sample and XMCD technique just probes a depth of a few nanometers.

Fig. 5b shows the normalized XMCD hysteresis-loops corresponding to ZFO1, all of them normalized by their values at 0.6 T.

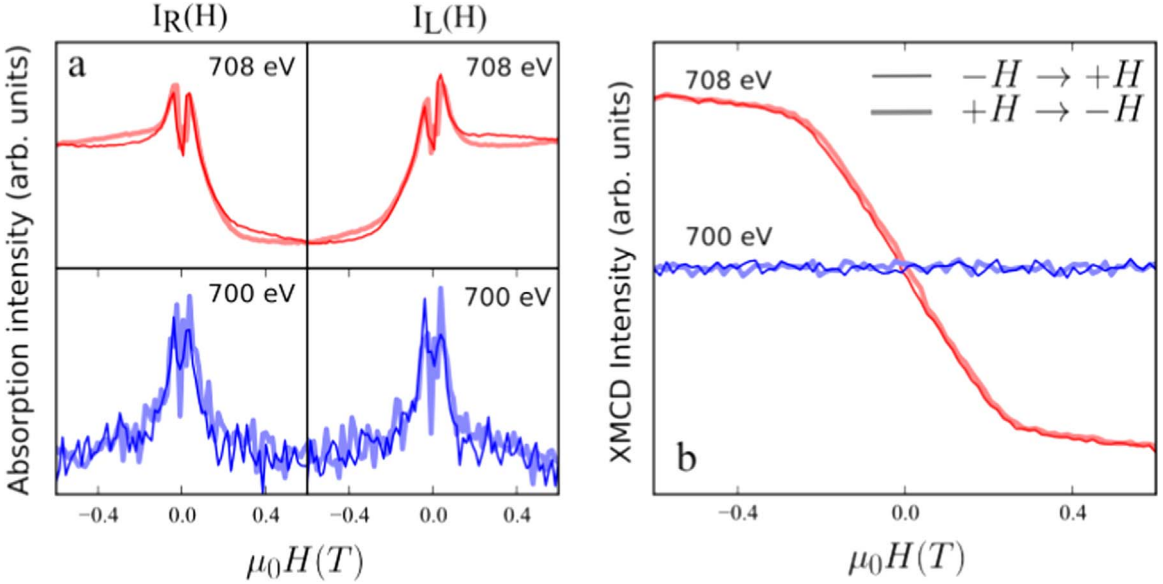

Fig. 3. Measures corresponding to ZFO1 film. a) $I_R(H)$ and $I_L(H)$ signal obtains (average over eight measurements) for X-ray energy fixed at 708 eV (P_{B1} Peak) and 700 eV (background). b) XMCD hysteresis-loops obtained as $I_R(H)$–$I_L(H)$ both for P_{B1} and background. In all cases the positive (negative) values of $\mu_0 H$ correspond to magnetic field parallel (antiparallel) and thin (thick) line correspond to experiment perform from negative to positive (positive to negative) values of $\mu_0 H$ to the propagation vector direction.

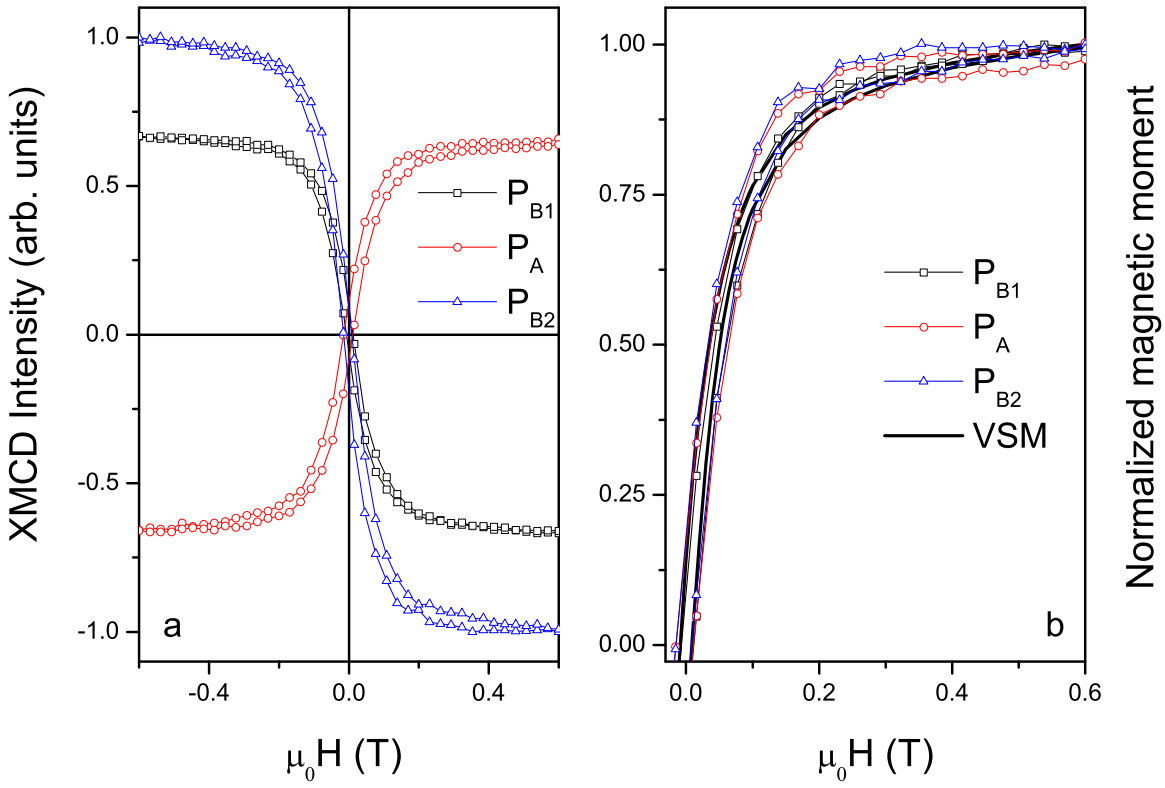

Fig. 4. a) XMCD hysteresis-loops of maghemite nanoparticles at the photon energies marked with P_A, P_{B1} and P_{B2} in the XMCD spectrum of Fig. 1. The positive (negative) values of $\mu_0 H$ correspond to magnetic field parallel (antiparallel) to the propagation vector direction. b) XMCD hysteresis-loops of Fig. 3a and magnetization curve measured with VSM of maghemite nanoparticles, all of them normalized by its value at $\mu_0 H = 0.6$ T.

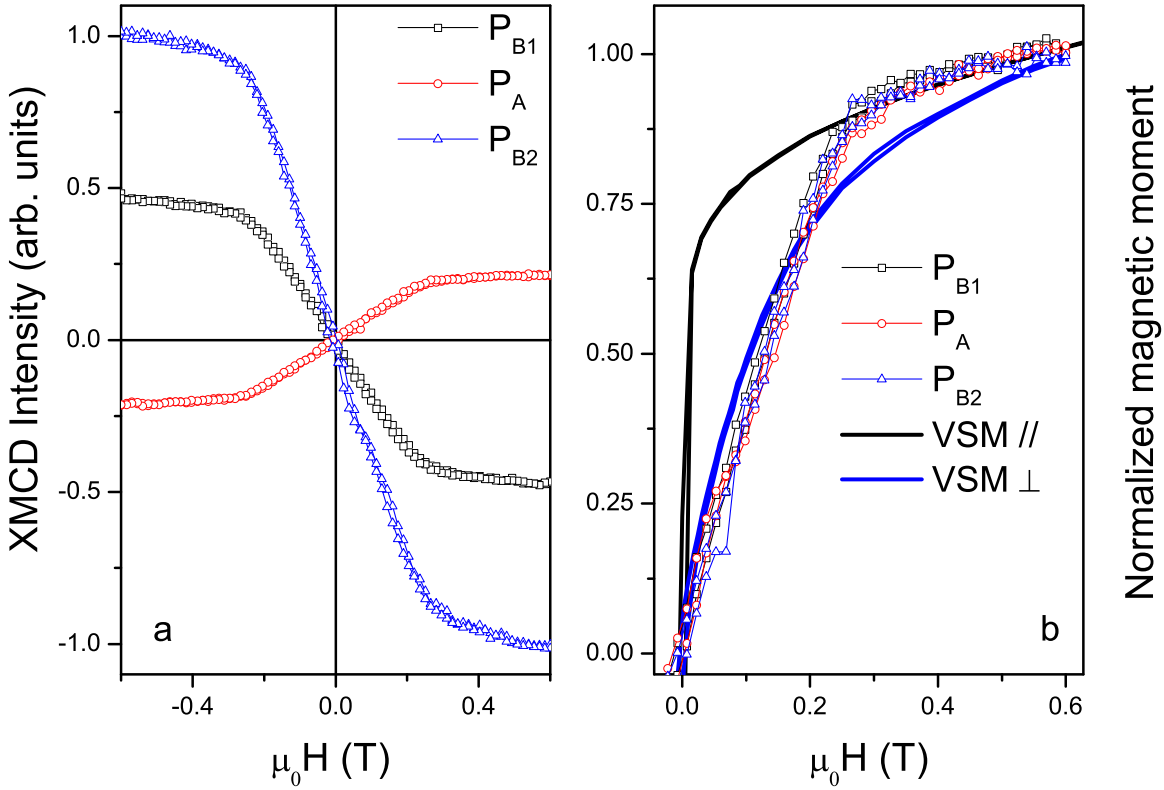

Fig. 5. a) XMCD hysteresis-loops of ZFO1 at Fe L_3-edge corresponding to Fe_A^{3+} (P_A) and Fe_B^{3+} (P_{B1} and P_{B2}) normalized by its value at $\mu_0 H = 0.6$ T. The positive (negative) values of $\mu_0 H$ correspond to magnetic field parallel (antiparallel) to the propagation vector direction. The sample plane is perpendicular to the direction of the photon propagation-vector and of the magnetic field. b) XMCD hysteresis-loops of Fig. 4a and magnetization curve of ZFO1 measured with VSM magnetic field direction both on the plane of the sample (parallel symbol) and perpendicular to the plane of the sample (perpendicular symbol). All of them are normalized by its value at $\mu_0 H = 0.6$ T.

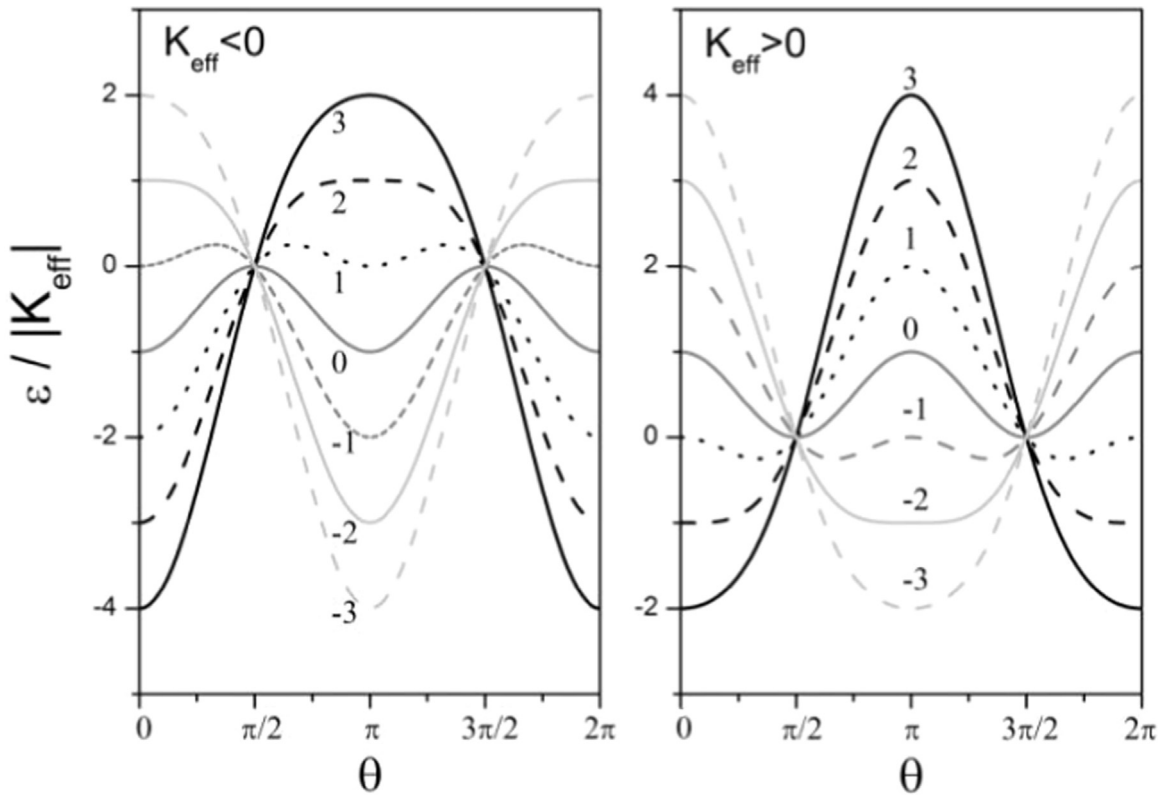

Fig. 6. Reduced magnetic energy density as a function of the angle θ for different γ values (indicated for each curve en the figure). The cases of negative and positive K_{eff} are shown.

VSM hysteresis-loops measured with magnetic field perpendicular and parallel to the film plane are also included for comparison purposes. In the case of the VSM hysteresis-loops, it was necessary to subtract the diamagnetic substrate contribution. The magnetic response of the whole sample, determined through the VSM measurements, reveals that the easy axis of magnetization is in the sample plane.

In XMCD hysteresis-loops, the perfect coincidence of specific contributions from Fe^{3+} at A- and B-sites can be observed. The XMCD hysteresis-loops have almost zero coercivity and remanence. The hysteresis-loops shape, measured under the same geometry conditions, obtained with both XMCD and VSM for the ZFO1 sample present significant differences, in contrast to the magnetic nanoparticles sample loops, which are identical. These differences reveal that the sample presents distinctive magnetic responses in the film surface region and in the film interior region XMCD mean probing depth (λ) is few nanometers while VSM is sensitive to the whole sample. For the case of magnetic iron oxides $\lambda \approx 5$ nm [21].

In the next section we considered the energy contributions that determine the moment orientations in the surface layer of depth λ.

4. Uniaxial magnetic anisotropy

Magnetic anisotropy energy in thin film could be separated in a volume contribution K_v (J/m^3) and a contribution from surfaces K_s (J/m^2). Reduced local symmetry at surfaces and interfaces results in a magnetic contribution to the surface energy depending on the orientation of spontaneous magnetization $\mathbf{M_s}$. This magnetic contribution to the energy was called magnetic surface anisotropy by Néel [22]. Assuming Néel's ideas valid in the present case, the first order contribution term to the energy depends on the angle θ between the orientation of the spontaneous magnetization $\mathbf{M_s}$ and the surface normal (which is the same angle in every domain since field is applied in the normal direction) as:

$$E_{Ks}(\theta) = AK_s\cos(\theta)^2, \quad (1)$$

where K_s is the surface anisotropy constant and A the area of the sample. The energy related with the volume anisotropy in the case of in-plane anisotropy becomes $E_{Kv}(\theta) = \lambda\, A\, K_v \cos(\theta)^2$,

In presence of an applied magnetic field ($\mu_0\mathbf{H_a}$) we also have to consider both the Zeeman energy and the demagnetizing field energy contributions. When **H** is applied perpendicular to the film plane, as in our XMCD measurements, the component of magnetization in the surface normal direction is the same at any place of the sample surface. Hence the Zeeman energy is given by:

$$E_Z(\theta) = -\mu_0\lambda A\mathbf{M_s}.\,\mathbf{H_a} = -\mu_0\lambda A M_s H_a\cos(\theta) \quad (2)$$

and the demagnetizing field energy contribution is:

$$E_d(\theta) = \tfrac{1}{2}\mu_0\lambda A\mathbf{M_s}.\,\mathbf{H_d} = \tfrac{1}{2}\mu_0\lambda A M_s H_d\cos(\theta) \quad (3)$$

where $\mathbf{H_d}$ is the demagnetizing field. If $N_\perp$ is the demagnetizing factor in the direction perpendicular to the film plane, the magnitude of the demagnetizing field is $H_d = N_\perp M = N_\perp M_s \cos(\theta)$. Thus considering all magnetic anisotropy contributions and defining the effective anisotropy constant $K_{eff} = K_s/\lambda + K_v + \tfrac{1}{2}\mu_0 N_\perp M_s^2$ the total energy can be written as:

$$E(\theta) = \lambda A\, K_{eff}\cos^2(\theta) - \mu_0\,\lambda\, A\, M_s\, H_a\cos(\theta) \quad (4)$$

Finally, defining the dimensionless parameter $\gamma = \mu_0 M_s H/|K_{eff}|$, the volume energy density $\varepsilon = E/(A\,\lambda)$ can be written as:

$$\varepsilon(\theta) = |K_{eff}|\left(\pm\cos^2(\theta) - \gamma\cos(\theta)\right),$$

where the $+$ $(-)$ sign corresponds to $K_{eff} > 0$ ($K_{eff} < 0$). For positive K_{eff} and no applied field, i.e. $\gamma = 0$, the volume energy density ε_s is lowest for parallel to the surface orientation of the

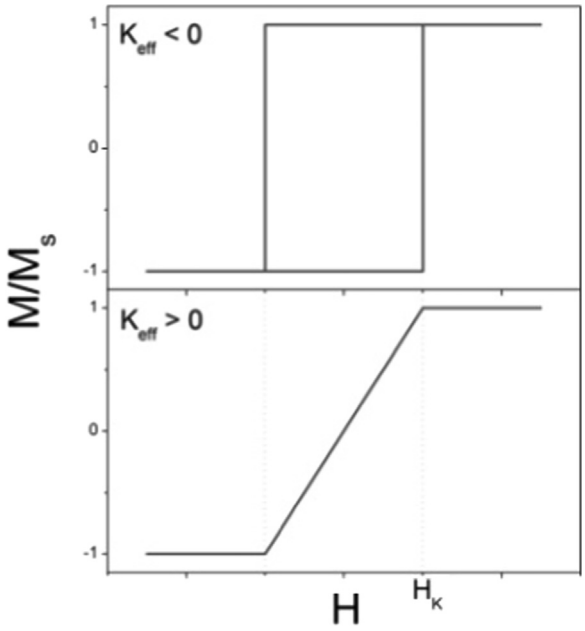

Fig. 7. Hysteresis-loops predicted for K_{eff} negative and positive values from magnetic energy density.

magnetization. Reduced magnetic energy density as a function of the angle θ for different γ values is shown in Fig. 6.

The minima of the magnetic energy density determine the equilibrium direction (θ_{min}) of the spontaneous magnetization. When $K_{eff} < 0$, the energy profile displays minima at $\theta = \pi$ for $\gamma < 2$ and at $\theta = 0$ for $\gamma > -2$, that is at the directions corresponding to magnetic saturation along the field direction. When $K_{eff} > 0$, the energy profile displays minima at $\theta = 0$ and $\theta = \pi$ for $\gamma > 2$ and $\gamma < -2$, respectively; and at $\cos(\theta) = \gamma/2$ for $|\gamma| < 2$. Hence, different magnetic hysteresis-loops are predicted for K_{eff} negative and positive values, which can be obtained as $M(H) = M_s \cos(\theta_{min})$ (see Fig. 7). In this framework, it is possible to define the anisotropy field H_K as the field corresponding to $\gamma = 2$, that is $\mu_0 H_K = 2K_{eff}/M_s$.

The comparison of XMCD hysteresis-loops of ZFO1 at Fe L_3-edge of Fe^{3+} at A-sites and B-sites, with those predicted for samples with both negative and positive K_{eff} (Fig. 7) reveals that this material has positive K_{eff}. The anisotropy field value obtained from the XMCD hysteresis-loops is $H_K = 199$ kA/m ($\mu_0 H_k = 0.25$ T). As can be noted in Fig. 5b, the magnetization does not reach the saturation value at H_K field. The magnetization at this field is 100 kA/m. This value is lower than the magnetic saturation $\mathbf{M_s}$ = 140 kA/m obtained from VSM hysteresis-loop (not shown here) with maximum magnetic field strength $\mu_0 \mathbf{H} = 1.8$ T. Finally, it is possible to determine $K_{eff} = 12.6$ kJ/m^3.

As it was mentioned, when the magnetic response of the whole sample is measured, like in VSM measurement, magnetic anisotropy K_V determines the magnetic response since the effects of K_S can be disregarded. This fact allows the determination of K_V from VSM magnetization curves calculating the difference in energy W necessary to saturate the magnetization along the easy and hard directions corresponding to magnetic field along the plane of the sample (parallel symbol) and perpendicular to the plane of the sample (perpendicular symbol), respectively:

$$K_V = W_\perp - W_\parallel = \mu_0 \int_0^{M_S} H_\perp dM - \mu_0 \int_0^{M_S} H_\parallel dM$$

Considering the demagnetizing field $\mathbf{H}_d = -N_\perp \mathbf{M}$ and the relation $\mathbf{H}_\perp = \mathbf{H}_{a\perp} - N_\perp \mathbf{M}$ (and similar equation for parallel direction) is possible to obtain the following expression for K_V as function of the applied field:

$$K_V = \mu_0 \int_0^{M_S} H_{a\perp} dM - \mu_0 \int_0^{M_S} H_{a\parallel} dM - \frac{1}{2}(N_\perp - N_\parallel)\mu_0 M_s^2$$

Considering the sample geometry and dimension, the demagnetizing factor are $N_\perp \approx 1$ and $N_\parallel \approx 0$ [23]. The K_V value obtain by this method is 3.1 kJ/m^3. Finally, knowing K_V is possible to determine the surface anisotropy contribution to K_{eff}, $K_s/\lambda = 3.2$ kJ/m^3 and $K_S = 16$ μJ/m^2 (1.6×10^{-2} erg/cm^2).

5. Summary

In this work we study the surface magnetic response in zinc ferrite ($ZnFe_2O_4$) thin film (thickness t~57 nm) by X-ray Magnetic Circular Dichroism (XMCD) performed in the TEY mode and analyze the results in terms of the surface magnetic anisotropy. We performed measurements of magnetic moment vs. applied field cycles via XMCD. The selective nature of the X-ray spectroscopy allowed the determination of the magnetic behavior of iron 3+ at each site (tetrahedral and octahedral), separately. The perfect coincidence of magnetic contributions from Fe^{3+} at A- and B-sites allows confirming that both sites correspond to the same magnetic phase. Results show that iron in octahedral and tetrahedral sites of spinel structure are coupled antiferromagnetically between them, and when magnetic field is applied the magnetic moment of the ion located at octahedral sites align along the field direction.

Since XMCD probing depth in TEY mode is $\lambda \approx 5$ nm for magnetic iron oxides, it is possible to determine the surface magnetic contribution combining this technique with VSM measurements which are sensitive to the whole sample. The magnetic measurements reveal a distinctive response of the surface with in-plane anisotropy and an effective anisotropy constant value of 12.6 kJ/m^3. Through VSM measurements, a volume magnetic anisotropy K_V of 3.1 kJ/m^3 is determined. Finally, using these results a surface magnetic anisotropy K_S of 16 μJ/m^2 is determined.

Acknowledgment

We appreciate financial support by LNLS (PGM 12490), Campinas, SP, Brazil (proposals SGM and PGM 12490); CONICET (PIP 1111 and PIP 0324); ANPCyT, Argentina (PICT 1399-2008, PICT 2010-2721 and PICT 2010-2785).

References

[1] S.J. Stewart, S.J.A. Figueroa, J.M. Ramallo López, S.G. Marchetti, J.F. Bengoa, R. J. Prado, F.G. Requejo, Phys. Rev. B 75 (2007) 073408.
[2] C.N. Chinnasamy, et al., J. Phys.: Condens. Matter 12 (2000) 7795.
[3] J. Smit, H.P.J. Wijn, Ferrites, Philips Technical Library, Eindhoven, 1959.
[4] J. Smit, H.P.J. Wijn, Ferrites, Wiley, New York, 1959.
[5] W. Schiessl, W. Potzel, H. Karzel, M. Steiner, G.M. Kalvius, A. Martin, M. K. Krause, I. Halevy, J. Gal, W. Schäfer, G. Will, M. Hillberg, R. Wäppling, Phys. Rev. B 53 (1996) 9143.
[6] S.A. Oliver, H.H. Hamdeh, J.C. Ho, Phys. Rev. B 60 (1999) 3400.
[7] S. Nakashima, K. Fujita, K. Tanaka, K. Hirao, T. Yamamoto, I. Tanaka, Phys. Rev. B 75 (2007) 174443.
[8] V. Stevanović, M. d'Avezac, A. Zunger, Phys. Rev. Lett. 105 (2010) 75501.
[9] C.E. Rodríguez Torres, F. Golmar, M. Ziese, P. Esquinazi, S.P. Heluani, Phys. Rev. B 84 (2011) 064404.
[10] Y.F. Chen, D. Spoddig, M. Ziese, J. Phys. D: Appl. Phys. 41 (2008) 205004.
[11] C. Rodriguez Torres, et al., Phys. Rev. B 89 (2014) 104411.
[12] G. van der Laan, J. Phys.: Conf. Ser. 430 (2013) 012127.
[13] B.T. Thole, P. Carra, F. Sette, G. van der Laan, Phys. Rev. Lett. 68 (1992) 1943.
[14] J. Sthör, J. Magn. Magn. Mater. 200 (1999) 470.
[15] J.S. Kang, G. Kim, H.J. Lee, D.H. Kim, H.S. Kim, J.H. Shim, S. Lee, Hangil Lee, J.-Y. Kim, B.H. Kim, B.I. Min, Phys. Rev. B 77 (2008) 035121.
[16] G. van der Laan, A.I. Figueroa, Coord. Chem. Rev. 277 (2014) 95.
[17] C.T. Chen, Y.U. Idzerda, H.-J. Lin, N.V. Smith, G. Meigs, E. Chaban, G.H. Ho, E. Pellegrin, F. Sette, Phys. Rev. Lett. 75 (1995) 152.
[18] S. Brice-Profeta, et al., J. Magn. Magn. Mat. 288 (2005) 354.

[19] J.J.S. Figueiredo, R. Basilio, R. Landers, F. Garciab, A. de Siervo, J. Synchrotron Radiat. 16 (2009) 346.
[20] J.P. Crocombette, M. Pollak, F. Jollet, N. Thromat, M. Gautier-Soyer, Phys. Rev. B 52 (1995) 3143.
[21] S. Gota, et al., Phys. Rev. B 62 (2000) 4187.
[22] L. Néel, L'anisotropie superficielle des substances ferromagnetiques, C.R. Acad. Sci. Paris 237 (1953) 1468.
[23] A. Aharoni, J. Appl. Phys. 83 (1998) 3432.